

Hyperspectral Imagery Visualization Using Double Layers

Shangshu Cai, *Student Member, IEEE*, Qian Du, *Senior Member, IEEE*, and
Robert J. Moorhead, II, *Senior Member, IEEE*

Abstract—Displaying the abundant information contained in a hyperspectral image is a challenging problem. Almost any visualization approach reduces the information content. However, we want to maximize the amount of object or material information presented. A visualization approach that uses classification as an intermediate step may maximize the information transfer. In our research, we are particularly interested in the display of mixed-pixel classification results, since most pixels in a remotely sensed hyperspectral image are mixed pixels. In this paper, we propose a visualization technique that employs two layers to integrate the mixture information (i.e., endmembers and their abundances) in each pixel. Images can be displayed with any desired level of details.

Index Terms—Hyperspectral imagery visualization, linear unmixing analysis, unsupervised classification.

I. INTRODUCTION

A HYPERSPECTRAL imaging sensor uses hundreds of coregistered channels to acquire images of the same area on the Earth. It provides high-resolution spectral information to enable more accurate material detection, classification, identification, and quantification. However, it is challenging to display the abundant information contained in such a 3-D image cube. There exist two major categories in visualization: one is to represent as much data information as possible, and the other is to use the human perceptual channels ergonomically. In this paper, we focus on the methods in the first category.

False-color images, which map three spectral channels into three RGB channels, have been used to display multispectral remotely sensed images for decades. For instance, a color infrared composite, which provides a quick overview of the materials in a scene, is a typical method to display multispectral data [1]. Robertson and O'Callaghan suggested using a linear transformation to project the original bands into three channels and then to map the three channels to a perceptual color space to achieve high contrast image [2]. Durand and Kerr selected three channels and balanced the signal-to-noise ratio (SNR) to obtain an enhanced color contrast image [3]. When displaying hyperspectral imagery, these methods may not be sufficient to visualize the information contained in hundreds of spectral channels.

Manuscript received September 29, 2006; revised December 4, 2006. This work was supported by NASA Science Mission Directorate, Applied Sciences Program as part of a Crosscutting Solutions contract to Mississippi State University through the Stennis Space Center.

The authors are with the Department of Electrical and Computer Engineering and the GeoResources Institute in the High Performance Computing Collaborative (HPC²), Mississippi State University, Mississippi State, MS 39762 USA.

Digital Object Identifier 10.1109/TGRS.2007.894922

One of the solutions in the hyperspectral imagery display is to condense the information into three major channels and map it to the RGB color space. A typical method is to display the first three principal components (PCs) from PC analysis (PCA) [4]. However, the original PCA method does not balance the SNR well. Moreover, lots of information including interesting object information may be present in other PCs. Therefore, a noise-adjusted PCA (NAPCA) may be a better choice. A PCA-class method for color display has been presented for the hyperspectral image display [5], [6]. In the work of Jacobson and Gupta [7], fixed linear spectral weighting envelopes were introduced to create a natural-looking imagery that displays the same materials in different datasets consistently. However, these unsupervised transformation-based techniques result in the loss of information, including objects.

Another way to exhibit hyperspectral images is to visualize the classification results. In pure-pixel classification, a false-color display, which assigns a color label to each class, can be used [8]. Since most pixels are mixed in a remotely sensed hyperspectral image due to a low spatial resolution, it is more useful to conduct a mixed-pixel classification. In mixed-pixel classification, a pixel has a certain percentage of each class. Traditionally, one displays the resulting grayscale classification maps separately and views them side by side, making it difficult to build the spatial relationship among classes. It is also impossible to perceive the contents within a single pixel. A visualization system was developed by Wessels *et al.* [9], in which the pixel color was assigned to be the color of the most abundant class, but other class information was suppressed.

It should be noted that the visualization of classification result can be considered a multivariate visualization problem. This problem has been studied for many years [10]–[12]. In [10], discrete and continuous visual elements were combined to visualize multiple fields on a surface. Texture mapping and 3-D surface shape were employed to display multivariate data in [11]. Bokinsky used different sizes and distributions of dots to represent different variables [12]. All of these methods take the multivariates as independent variables, and no relationship exists among them because they are different physical quantities.

According to our *ad hoc* study, color display using classification result generally can produce better data analysis performance than one that uses a simple data transformation. Thus, in this paper, we investigate how to effectively visualize the mixed-pixel classification results. We present a new approach that employs two layers to visualize the mixed-pixel information with different levels of details. This approach takes

TABLE I
NUMBER OF BANDS BEFORE AND AFTER AUTOMATIC SELECTION

Dataset	Original	After Selection
AVIRIS Lunar Lake	224	158
AVIRIS Low Altitude	224	132
Hyperion	220	152

advantage of the classification result from fully constrained linear unmixing, such as the technique in [13]. At the very detailed level, it displays pixel composition at the subpixel level. On the other hand, it can display the overall material distribution in the image scene. Viewers can choose any detail level for information display. Based on this double-layer scheme, a visualization system with interactive tools is developed.

This paper is organized as follows. Section II provides the details on hyperspectral image processing and analysis. In Section III, the color mapping strategies and double-layer visualization approach are presented. In Section IV, the developed hyperspectral image visualization interface is introduced. Three visualized examples are shown in Section V. Section VI draws the conclusion.

II. DATA PROCESSING AND ANALYSIS

Preprocessing or data preparation is a necessary part of the visualization process. A hyperspectral image may contain some bad bands, such as water absorption and low SNR bands, and bad pixels, such as white spots due to sensor saturation. These bad bands and bad pixels impact the data analysis. Before classification, they need to be automatically removed.

A. Removal of Bad Bands

A hyperspectral image has high spectral correlation. Thus, two adjacent bands tend to have very high correlation. The bands that are not similar to their neighbors may contain a high level of noise. Due to low reflectance, noise plays a key role in water absorption bands. Therefore, the correlation between adjacent water absorption bands is also very low. These facts are used to automatically remove all these unwanted bands. The detailed steps are as follows.

- 1) Compute the correlation coefficient between each pair of bands.
- 2) For each band, compare the correlation coefficients with the neighboring channels. If both of the correlation coefficients are greater than a given threshold η , this band is kept; otherwise, it is removed as a bad band.

Table I lists the bad-band removal result for three datasets with the threshold $\eta = 0.8$. The high quality of bands selected demonstrates that this approach can efficiently remove the water absorption and low SNR bands, and the result is very close to that from manual selection.

B. Removal of Bad Pixels

Due to sensor noise, some bad pixels may occur in a selected band. Two types of noise may exist: isolated pixels and striping

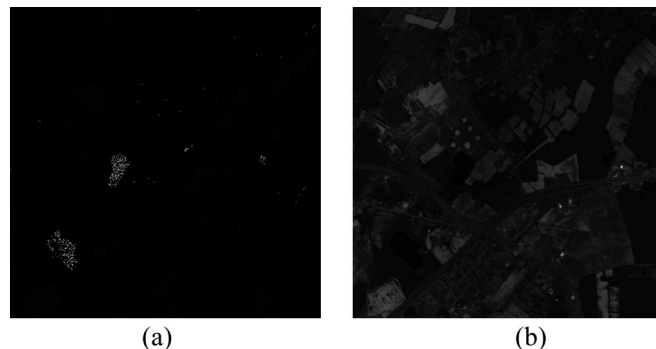


Fig. 1. Band 173 in the AVIRIS low altitude data (a) before bad pixels are removed and (b) after bad pixels are removed.

lines. An isolated noisy pixel is not spatially or spectrally correlated with the neighboring pixels. The pixels in a noisy line are correlated. Thus, different algorithms are used to remove isolated pixels and lines.

1) *Removal of Isolated Noisy Pixels*: A lowpass filter can smooth out the isolated noisy pixels, but it will also blur the normal pixels. In order to reduce the impact to the normal pixels when removing the abnormal pixels, an algorithm with the following steps is applied.

- 1) Find the maximum pixel value in the band.
- 2) Find the pixels whose values are greater than a certain percentage (λ_1) of the maximum value, and take these pixels as abnormal pixel candidates.
- 3) Check the value of the abnormal pixel candidates in the adjacent bands. If the pixel value exceeds the maximum value of the same pixel in the adjacent bands by a certain percentage (λ_2), it is considered as a bad pixel.
- 4) Conduct the signature interpolation and use the interpolated values to replace the bad pixels.

In practice, $\lambda_1 = 80\%$ and $\lambda_2 = 90\%$ can achieve good results. The spectral inspection in Step 3) is particularly important to avoid accidentally removing those normal pixels with large reflectance. Fig. 1 displays Band 173 in the Airborne Visible/Infrared Imaging Spectrometer (AVIRIS) low-altitude imagery before and after bad pixel removal. Fig. 1(a) is dark because some isolated pixel values are so large that they suppress the brightness of other pixels. Fig. 1(b) is the image after the bad pixels have been removed, where image content becomes visible.

2) *Removal of Dark or White Noisy Lines*: Stripe patterns may exist in some bands [14]. The algorithm to automatically remove a dark line with the Hough transform [15] has the following steps.

- 1) Compare each pixel with its four closest neighbors. If its value is less than ε , for example, 80%, of the neighborhood average, mark this pixel as a bad pixel candidate.
- 2) Create a binary image where the pixels corresponding to the bad pixel candidates are set to 1 and others 0.
- 3) Detect lines across the entire binary image using the Hough transform. The candidates that are located in the detected lines are considered as bad pixels.
- 4) Interpolate and replace the bad pixels along the detected lines.

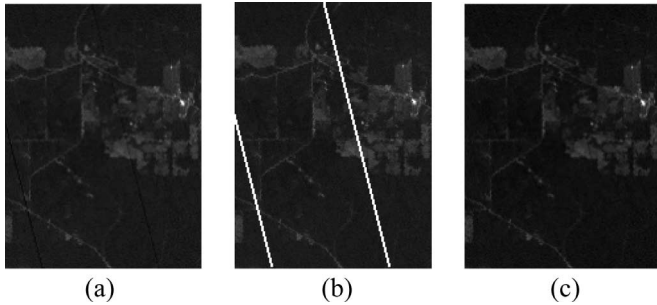


Fig. 2. Band 10 of Hyperion data. (a) Original image, (b) detected stripes, and (c) after the stripes are removed.

As shown in Fig. 2, the line noise can be effectively detected and removed. This algorithm can be easily modified to detect white line noise.

C. Linear Mixture Analysis

Linear mixture analysis is a widely used method to classify and quantify multispectral/hyperspectral imagery. Each pixel in the hyperspectral imagery can be represented as a vector \mathbf{r} whose dimension is $l \times 1$, where l is the number of spectral bands. Assume that the number of endmember materials is n . Let \mathbf{M} be the signature matrix of these materials denoted as $\mathbf{M} = [\mathbf{m}_1, \mathbf{m}_2, \dots, \mathbf{m}_n]$, where \mathbf{m}_j is an $l \times 1$ vector corresponding to the signature of the j th material. According to the linear mixture model, the pixel \mathbf{r} can be represented as

$$\mathbf{r} = \mathbf{M}\boldsymbol{\alpha} + \mathbf{n} \quad (1)$$

where $\boldsymbol{\alpha} = (\alpha_1 \dots \alpha_i \dots \alpha_n)^T$ is an $n \times 1$ column vector called the abundance vector, whose i th element represents the proportion of the i th endmember material in the pixel \mathbf{r} . Here, \mathbf{n} represents an additive noise or sensor measurement error.

Since $\boldsymbol{\alpha}$ represents endmember abundance, α_i for $1 \leq i \leq n$ should be a positive value. Also, the whole pixel is constructed by all the endmembers. Hence, their sum should be one. These two constraints can be formed as

$$\sum_{i=1}^n \alpha_i = 1 \quad 0 \leq \alpha_i \leq 1. \quad (2)$$

When the \mathbf{M} is known, a constrained optimization problem can be imposed to estimate $\boldsymbol{\alpha}$ that yields the minimum estimation error when the constraints in (2) are satisfied, which is referred to as fully constrained least squares linear unmixing (FCLSLU). It can simply be achieved by using a quadratic programming. If \mathbf{M} is unknown, then unsupervised FCLSLU needs to be performed [13], whose procedure can be described as follows.

- 1) Select the two pixels with the maximum and minimum norms from the image and construct $\mathbf{M} = [\mathbf{m}_1, \mathbf{m}_2]$. Then, use the quadratic programming to solve $\boldsymbol{\alpha} = [\alpha_1, \alpha_2]$.
- 2) Calculate the reconstruction error e between the pixel vector \mathbf{r} and its estimate, i.e., $e = \|\mathbf{r} - \mathbf{M}\boldsymbol{\alpha}\|$.

- 3) Find the pixel that has the maximum error and take it as a third endmember, i.e., $\mathbf{M} = [\mathbf{m}_1, \mathbf{m}_2, \mathbf{m}_3]$. Then, use the quadratic programming again to estimate the abundances in the new $\boldsymbol{\alpha}$.
- 4) Repeat Steps 2) and 3) for additional endmembers and their abundances, until the error is less than a given threshold ξ or reach the maximum number of endmembers.

When the number of endmembers is unknown, a large number can be assumed first to run the unsupervised FCLSLU algorithm. Then, the similar endmember signatures can be combined after the similarity comparison using Spectral Angle Mapper (SAM), and the endmember signatures corresponding to noisy abundance images with large entropies can be removed. The remaining signatures are used for the supervised FCLSLU to generate the final abundance images for visualization.

III. DOUBLE-LAYER VISUALIZATION SCHEME

The resulting abundance images from the linear mixture analysis in Section II provide the spatial distribution of each endmember material in an image scene. Traditionally, each abundance image is displayed as a grayscale image [13]. If there are n endmember materials, then n grayscale abundance images will be generated. There are, at least, two drawbacks for visualizing the abundance images as separate grayscale images: 1) it is difficult for viewers to find the overall distribution of the n materials in the image scene; and 2) it is difficult for viewers to know the material composition at any specific location in the image scene.

Therefore, in our approach, we visualize the n abundance images in one single color image by employing double layers to overcome these two drawbacks. First, distinctive colors are determined for all the abundance images. Second, a final color image is formed by applying a double-layer visualization, where Layer I displays the general distribution of materials and Layer II displays the detailed composition of each pixel. The final image display is generated by overlaying Layer II on Layer I.

A. Color Assignment Strategies

In the study of color perception, one of the first mathematically defined color spaces is the CIE XYZ color space. It was derived from a series of experiments which showed that almost all of the colors can be represented by a linear combination of three basic spectral signatures (roughly red, green, and blue), which are taken as the three coordinates X , Y , and Z . However, the CIE XYZ system does not give a direct way of estimating color differences. It would be desirable if a distance on a chromaticity diagram corresponded to the degree of difference between two colors. The two uniform color spaces provided by CIE are CIE LAB and CIE LUV, where the perceptual distance approximately equals the Euclidean distance in these two color spaces [16], [17]. However, the difference and the appearance of color not only depend on the tristimulus but also heavily depend on the adapted state of viewers, the constancy

and contrast, and the temporal and spatial structures of the tristimulus. A real ideal uniform color space should involve these factors. Unfortunately, such an ideal color visual model is unavailable because these factors are very complex, and the viewer's environments are not predictable [17].

Healey addressed three criteria for color selection: color category, color distance, and linear separation [18], [22]. When the number of colors to be selected is less than ten, the color labels selected from the hue-saturation-value (HSV) color space can belong to different color categories [18], [19]. The HSV space is very similar to the CIE LUV space when $S = 1$ and $V = 1$. Although the HSV color space is not uniform, the colors in the slice are very close to being uniform. Thus, the color selection from the HSV space does not theoretically satisfy the three criteria, but it is very close. However, in some cases, even when distinctive colors have been assigned, the final color display result may not be as good as expected because color perception is nonlinear. It is also suggested by other researchers that the color selection will have good performance if a luminance (or lightness) dimension is separated from the chromatic dimensions [20].

Therefore, we will conduct a distinct color selection in the HSV color space with the goal that a color display should have the capability of conveying more information about the spatial relationship among objects or materials and make it easier to separate pixels into different classes [21]. In some cases, experienced analysts may have a preknowledge about the classes and want to assign a specific color to a class. For instance, one may want to use green to display healthy vegetation. Therefore, two automatic color assignment strategies are developed: one with class similarity constraint only and one with both class similarity and color consistency constraints.

1) *Automatic Color Assignment With Class Similarity Constraint*: The endmembers determined in Section II can be arranged in a sequence based on their signature similarity using a metric such as SAM. Without loss of generality, assume that the endmembers matrix $\mathbf{A} = [\alpha_1, \dots, \alpha_i, \dots, \alpha_n]$ are arranged according to signature similarity, i.e., α_i is more similar to α_{i+1} than to α_{i+2} . To relax the similarity constraint in color assignment, the color for the i th abundance image corresponding to α_i is less similar to the $(i + 1)$ th image than to the $(i + 2)$ th.

In the HSV color space, hue is an angle between 0° and 360° , and each angle corresponds to a specific color tone. In order to choose the colors as distinctively as possible, the angles of hues are uniformly selected from $[0^\circ, 360^\circ]$ for the n classes, with the saturation and value being 1.0. The n color labels can be represented as

$$\mathbf{CL}_j = \begin{cases} H_j = 360^\circ j/n \\ S_j = 1.0 \\ V_j = 1.0 \end{cases} \quad j = 0, \dots, n - 1. \quad (3)$$

In order to separate similar classes as far as possible, the color labels are assigned in an interleaved way. Let \mathbf{h}_i be the color vector in the HSV space for the i th class, for $i = 1, \dots, n$. Also,

let the color labels assigned to \mathbf{h}_i be denoted as \mathbf{CL}_{j_i} . The index j_i can be determined by

$$j_i = (j_{i-1} + \lceil n/2 \rceil) \bmod n \quad (4)$$

if \mathbf{CL}_{j_i} has not been assigned. Otherwise

$$j_i = ((j_{i-1} + \lceil n/2 \rceil) \bmod n) + 1. \quad (5)$$

Here, $\lceil n/2 \rceil$ chooses the largest integer that is less than or equal to $n/2$. j_1 can be any number between $(0, n - 1)$. But, in general, $j_1 = 0$. Fig. 3(a) shows the six color labels assigned to six classes using (4) and (5) where the correspondences are $\mathbf{h}_1 \leftarrow \mathbf{CL}_0$, $\mathbf{h}_2 \leftarrow \mathbf{CL}_3$, $\mathbf{h}_3 \leftarrow \mathbf{CL}_1$, $\mathbf{h}_4 \leftarrow \mathbf{CL}_4$, $\mathbf{h}_5 \leftarrow \mathbf{CL}_2$, $\mathbf{h}_6 \leftarrow \mathbf{CL}_5$.

2) *Automatic Color Assignment With Class Similarity and Color Consistency Constraints*: In this color assignment method, the viewer can define the colors of some abundance images for consistent rendering. For instance, green is an obvious choice for healthy vegetation. Also, if a standard signature library is available, the identities of some endmembers may be recognized, and then, their abundance images may be assigned consistent colors if desired. The colors for the rest of the abundance images can be assigned with the similarity constraints. It should be noted that it may be impossible to satisfy both class similarity and color consistency constraints for the entire set of abundance images because these two constraints are contradictory in most cases.

Assume that K ($0 < K < n$) color labels have been predefined for K classes. The K color labels divide the 360° hue slice into K intervals $(\pi_1 \dots \pi_k \dots \pi_K)$, where π_k is the interval between $[H_k, H_{k+1}]$. Those classes whose colors have not been predefined are determined by the following rules.

- 1) Arrange the rest of classes on the order of similarity.
- 2) Pick the next class to assign the color vector \mathbf{h} .
- 3) Find the maximum interval π_i and assign $H = (H_i + H_{i+1})/2$ as the hue component of \mathbf{h} . If more than one interval have the maximum π , then choose the one that results in the H which is farthest from that for the previous class in the sequence.
- 4) Redivide the 360° hue slice into $K + 1$ intervals.
- 5) Repeat 2)–4) until all the classes are assigned colors.

Fig. 3(b) shows the color labels assigned to six classes where Class 1 and 3 are predefined as blue and green, respectively.

After the colors have been assigned in the HSV color space, they are converted to the RGB color space so that they can be used in the next visualization steps and displayed on standard color monitors.

B. Layer I—Background Layer

Layer I, referred to as the background layer, is formed by preassigning a color to each of the n abundance images and merging them using a linear transformation. This layer gives the viewers the overall spatial distribution of endmembers.

1) *Pixel Color Generation*: Each pixel in the abundance images can be presented as a vector $\alpha = (\alpha_1 \dots \alpha_i \dots \alpha_n)^T$ constrained by (2). The color that is selected by the color

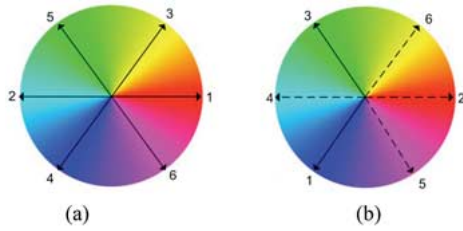


Fig. 3. Color assignment results. (a) Six classes are assigned color according to their signature similarity. (b) Class 1 and class 3 are predefined as blue and green, respectively.

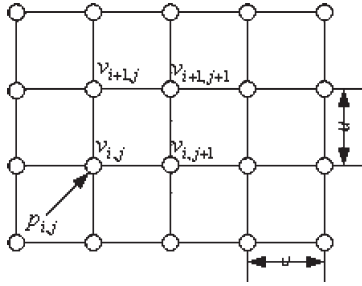


Fig. 4. Mapping scheme from pixels to vertices.

assignment strategies for the i th endmember can be denoted as $\mathbf{c}_i = (r_i \ g_i \ b_i)^T$ in the RGB color space. Then, a color matrix can be constructed as

$$\mathbf{C} = \begin{bmatrix} \mathbf{c}_1^T \\ \vdots \\ \mathbf{c}_i^T \\ \vdots \\ \mathbf{c}_n^T \end{bmatrix} = \begin{bmatrix} r_1 & g_1 & b_1 \\ \vdots & \vdots & \vdots \\ r_i & g_i & b_i \\ \vdots & \vdots & \vdots \\ r_n & g_n & b_n \end{bmatrix}. \quad (6)$$

The final color for the vector α in Layer I can be achieved by multiplying the pixel vector with the color matrix, i.e.,

$$\mathbf{c}^T = \alpha^T \mathbf{C}. \quad (7)$$

Since α was constrained by (2), the final color will be within the normal range $[0, 1]$ of color components.

2) *Mapping Pixels to Vertices*: OpenGL is a device-independent 3-D graphics library [23]. Setting a series of primitives in OpenGL can easily render 2-D or 3-D images. One of these primitives displays an OpenGL point with a size and color, which is referred to as vertex. A vertex can be considered a geometrical point with a given spatial position and color. A simple mapping function is formed from an image pixel to an OpenGL vertex as

$$f : p_{ij} \rightarrow v_{ij}. \quad (8)$$

Fig. 4 illustrates the mapping procedure. The vertical and horizontal distance between two adjacent vertices is u . Then, the mapping functions between p_{ij} and v_{ij} are represented as

$$\begin{aligned} p_{ij} \cdot \text{position} &= (i, j) \\ v_{ij} \cdot \text{position} &= (iu, ju) \\ v_{ij} \cdot \text{color} &= p_{ij} \cdot \text{color}. \end{aligned} \quad (9)$$

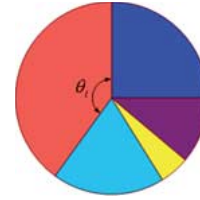


Fig. 5. Fan-shaped superpixel with its mixture composition.

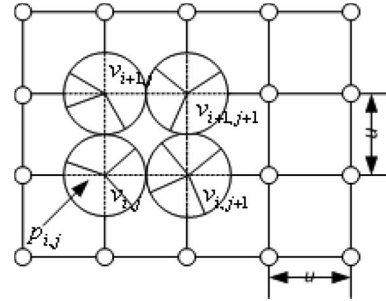


Fig. 6. Mapping function from pixels to superpixels.

Based on this mapping function, the color of vertices is determined by the color of the corresponding pixel, which is obtained by (7). The color of any point that is not a vertex will be determined by linearly interpolating the colors of the four closest vertices. The color of any point in this layer, including vertices and the intervening space, is denoted as C_I .

C. Layer II—Detail Layer

Layer II, referred to as the detail layer, introduces a “superpixel” to display the distribution detail of each endmember in a pixel at that position. Superpixel, also known as circle segments [24] and star maps [25], is a method to visualize multivariate data.

In this layer, each endmember is represented by a pie chart, as shown in Fig. 5. Without preknowledge about the classified endmembers, each member is considered as equally important. Therefore, an endmember is randomly assigned to the i th fan region. In general, the first endmember is chosen to assign the first region, and so on. The area of a fan-shaped region for the i th endmember is proportional to the angle θ_i , which is determined by its abundance α_i , i.e.,

$$\theta_i = \alpha_i \cdot 360^\circ. \quad (10)$$

Its starting and ending positions can be represented as

$$\beta_i^s = \sum_{j=1}^{i-1} \theta_j \quad \beta_i^e = \sum_{j=1}^i \theta_j \quad (11)$$

respectively. They can be related by $\theta_i = \beta_i^e - \beta_i^s$ and $\beta_1^s = 0^\circ$. Because α is constrained by (2), a pixel is shown as a full disk, i.e., $\beta_n^e = 360^\circ$.

Similar to the mapping in Layer I, Layer II maps a superpixel center to the corresponding vertex, and the radius of a superpixel is $u/2$ as shown in Fig. 6. The space in the pie chart will be filled by the color of the endmember that has been assigned

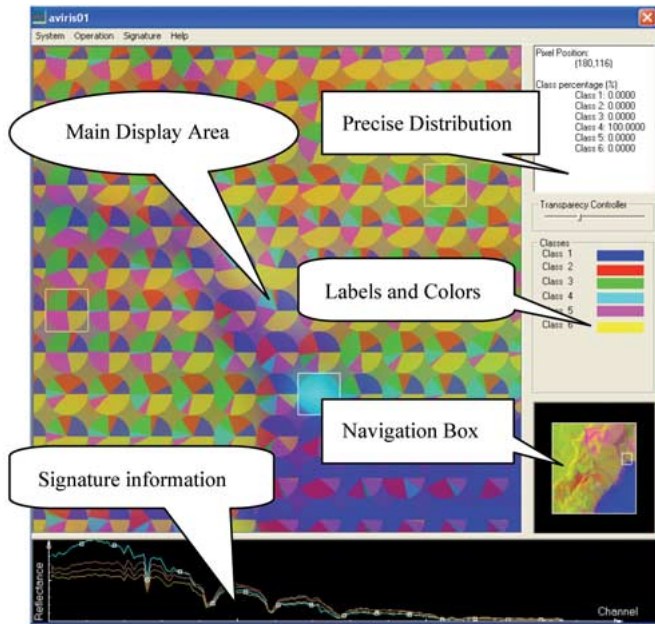


Fig. 7. Interface in the double-layer visualization system.

to this wedge. The color of the points that are not covered by the superpixels is set to black, i.e., $\mathbf{c} = [0, 0, 0]^T$. A color in Layer II is referred to as C_{II} .

D. Blending

After colors have been assigned to the two layers, Layer I, which gives the general distribution, and Layer II, which gives the details of the distribution, the final display can be generated. In order to display the two layers on the same device simultaneously, the color in the final image is determined by blending C_I and C_{II} . The blending is achieved by linearly combining C_I and C_{II} , which can be described as

$$C_{\text{final}} = t C_I + (1 - t) C_{II} \quad \text{for } 0 \leq t \leq 1. \quad (12)$$

Therefore, the color of the final image is within $[C_I, C_{II}]$. When t , the blending parameter, approaches 1, the final color trends to C_I , which means that the final image displays the general distribution information; when t is close to 0, the final color trends to C_{II} , which means that the final color image gives the detail distribution information.

IV. VISUAL EXPLORATION TOOLS

Visualization research has shown that interaction is a very efficient way to help viewers analyze data. In order to help viewers dig into the details of endmember distribution, the developed visualization system provides several interactive exploration tools to provide additional information in the main visual interface. The main visual interface, as shown in Fig. 7, is divided into five linked view areas: main display area, navigation display area, precise pixel information display area, signature information display area, and class labels and colors.

In the main display area, viewers can easily manipulate the visual result, such as zooming in, zooming out, and moving to

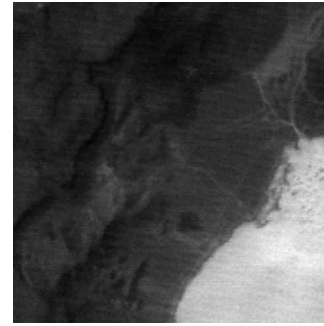


Fig. 8. AVIRIS Lunar Lake scene of size 200×200 .

select the region of interest (ROI) area. By selecting a ROI, one can obtain the desired degree of details. For example, by selecting a large area, Layer I will dominate the display, whereas the mixing details of each pixel are more visible if a small ROI is chosen. If a very small area is selected, the precise quantitative mixing information of each individual pixel can be seen. To avoid losing the spatial position when viewers select a very small ROI, a small navigation box is displayed to indicate the position of the ROI. Also, it can be used to change the ROI.

Although the distribution details can be revealed by Layer II, it may still be difficult for viewers to figure out the very precise distribution of endmembers. Therefore, the precise pixel information can be displayed, which includes the pixel position and exact abundances. Endmember signatures are always important in data analysis. Viewers can choose the spectral signatures to be shown, and the color of the signature is the same as the pixels in Layer I, which is also presented in the class color label area. Other information can be easily added to the visual interface.

V. EXPERIMENTS

Three examples are shown using the developed visualization system. They represent three different cases. The AVIRIS Lunar Lake scene to be visualized does not have noisy pixels; the AVIRIS low-altitude data are contaminated by isolated noisy pixels; and the Hyperion data contain lines that are noise. The two AVIRIS data are free downloads from the AVIRIS website (aviris.jpl.nasa.gov). The Hyperion data were obtained from the Earth Resources Observation Systems Data Center of the U.S. Geological Survey and in an area south of Mississippi State University.

The two color assignment strategies are used for these three examples. Because we have some prior knowledge about the AVIRIS Lunar Lake scene, the vegetation was preassigned to green. The rest of the class colors were automatically assigned based on the signature similarity. The second and third experiments implemented an automatic color assignment with the signature similarity constraint only, since no prior knowledge of the endmember types is available.

A. AVIRIS Lunar Lake Experiment

The AVIRIS Lunar Lake data, as shown in Fig. 8, were visualized by the proposed approach. After water absorption and low SNR bands were removed, 158 bands remained for

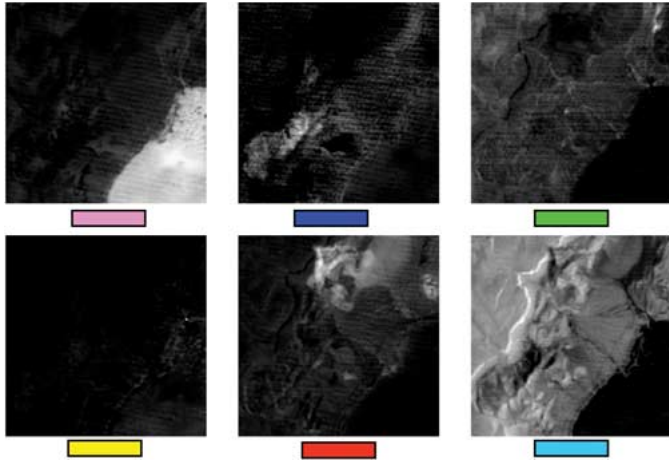


Fig. 9. Abundance images of the AVIRIS Lunar Lake and their assigned colors.

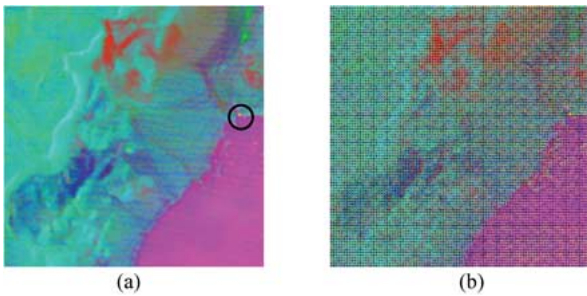


Fig. 10. Composite image based on the color assigned in Fig. 9. (a) Layer I. (b) Layer II.

processing. Fig. 9 shows the grayscale images of the six material abundances found by the unsupervised FCLSLU algorithm. In the abundance grayscale images, a bright pixel means that a large abundance of the specific material is resident in this location. Although the general distribution of one particular material is clearly displayed, it is difficult to visualize the constituent of a pixel.

Fig. 10 shows the Layers I and II images, in which each material was assigned the color indicated in Fig. 9. The right-most abundance image in the first row in Fig. 9 is vegetation; therefore, it was displayed in green. In Fig. 10(a), the six endmembers can be easily distinguished by color, such as magenta, blue, green, yellow, red, and cyan. In particular, an anomaly that is highlighted in the circle is displayed in yellow. Such a color display shows the overall material distribution and the fuzzy memberships of a pixel, but it cannot represent the detailed portions of materials within each pixel. For example, in the magenta area, it is difficult to see if other materials exist in this area and their portions. These cannot be resolved by only one layer. By introducing a second layer, as shown in Fig. 10(b), such detailed information can be revealed.

More details about the final color composite are shown in Fig. 11. The first column is the result when only Layer I was used to visualize the six endmembers, and the second column was generated when only Layer II was used. The third column is the result of blending the two layers with the specified values of t . On the other hand, the first row in Fig. 11(a) shows the

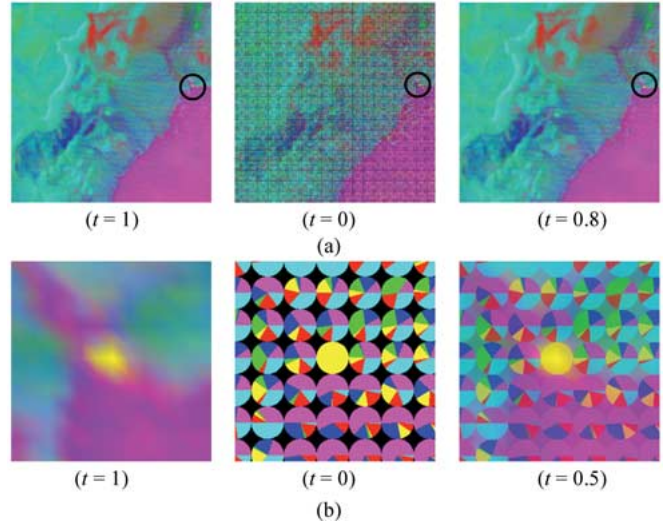


Fig. 11. Visualization results for the AVIRIS Lunar Lake data (from left to right: Layer I, Layer II, and double layers). (a) Overall images. (b) Details of pixels (the anomaly and its neighboring pixels).



Fig. 12. AVIRIS low-altitude scene of size 512×512 .

complete image using different values of t , and the second row in Fig. 11(b) zooms in on the ROI as highlighted in the first row where individual superpixel disks can be easily distinguished. As described in Section III, each disk represents a pixel, and the pie charts indicate the abundance of each material. In Fig. 11(b), we can easily see the anomaly pixel and its composition in the context of the neighborhood. This important information cannot be conveyed by viewing the original grayscale abundance images one after another.

This experiment clearly demonstrates the roles of Layer I and Layer II, and that, the double layers can effectively display the overall distribution and pixel composition details at the same time.

B. AVIRIS Low-Altitude Experiment

An AVIRIS low-altitude subimage with size of 512×512 , as shown in Fig. 12, was processed before visualization. One hundred thirty-two bands were kept after water absorption, and low SNR bands were removed. Isolated noisy pixels were removed using the algorithm in Section II-B. Without prior knowledge about this image scene, 30 materials were generated first, and seven meaningful material signatures were kept after abundance image selection and similar signature combination. Then, seven abundance images were produced by applying the

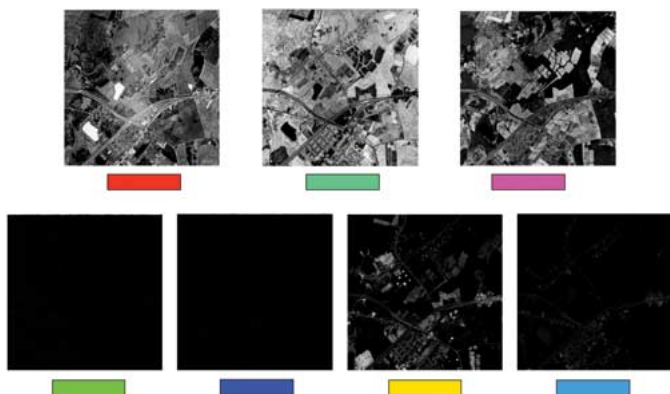


Fig. 13. Seven abundance images of AVIRIS low-altitude and their colors.

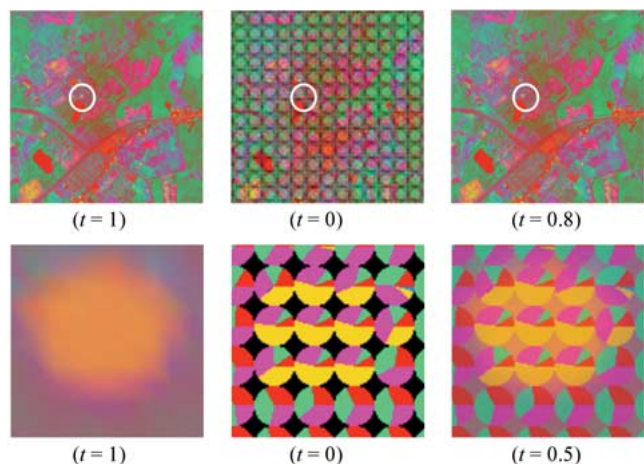


Fig. 14. Visualization results for the AVIRIS low-altitude data (from left to right: Layer I, Layer II, and double layers).

supervised FCLSLU. Fig. 13 displays these images and the automatically assigned colors.

Fig. 14 shows the final visualized images, such as Layer I (first column), Layer II (second column), and double layers (third column). The blending parameter t controls the amount of Layer I and Layer II in the final color display. The second row in Fig. 14 is about a ROI, a yellow spot, which is located in the white circle in the first row. Without using the double-layer display, viewers may be able to tell that this position contains some “yellow” material, but cannot gain a clear idea about its distribution. Our visualization system shows that the yellow spot not only contains this “yellow” material but also three other materials, and this material is the major component. The viewer can easily know the percentage of each material by looking at the top-right window, as shown in Fig. 7.

C. Hyperion Experiment

The Hyperion data, as shown in Fig. 15, were used to test the system as well. After water absorption and low SNR bands were removed, 152 bands remained. As the first spaceborne hyperspectral sensor, the images it produces contain lots of sensor noise such as dark lines. These dark lines greatly affect the classification results; therefore, the algorithm in Section II-B was employed to detect and remove these dark lines. After

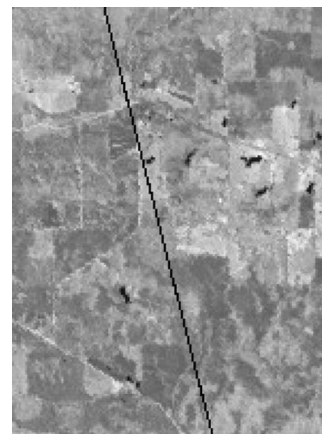


Fig. 15. Hyperion image scene of size 150×200 .

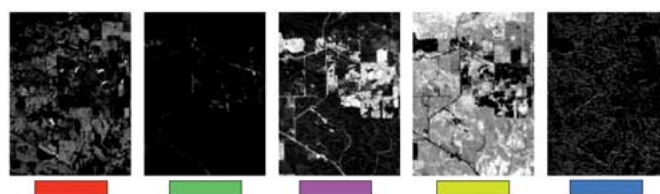


Fig. 16. Five abundance images of the Hyperion data and their colors.

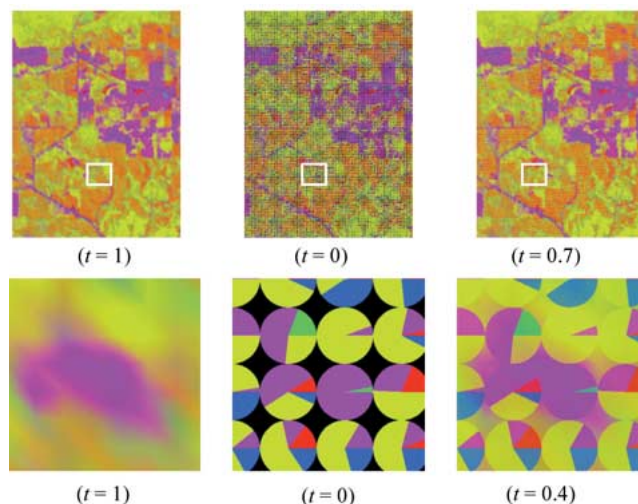


Fig. 17. Visualization results for the Hyperion data (from left to right: Layer I, Layer II, and double layers).

the dark lines were removed, 20 materials were extracted first using the unsupervised FCLSLU. Then, five signatures were kept after the selection of meaningful abundance images and combination of similar signatures. The five abundance images generated by the supervised FCLSLU and the automatically assigned colors are shown in Fig. 16.

Fig. 17 shows the color visualization comparison among the Layer I, Layer II, and double layers. For example, the distribution of the material in purple, corresponding to the buildings and roads, is easily seen in the first row; the small purple area highlighted in the first row is displayed as the ROI in the second row where we can see that none of the pixels is pure, and the largest abundance is about 90%. This experiment

further demonstrates that by using double layers, we can display both the general and detailed information as needed.

VI. CONCLUSION

This paper presents a novel approach to visualize hyperspectral remote sensing images by employing double color layers. It is an improvement from the conventional grayscale display that needs to show several grayscale images one after another, and it is also an improvement from other color displays that only give the general distribution of the endmembers. The proposed double-layer visualization technique can simultaneously display the overall endmember spatial distribution and their composition at the subpixel level. This technique is based on the unsupervised linear unmixing result, where noise and interference in the original image have been well presuppressed. It is particularly useful when the subpixel information is of interest. For example, by using the developed visualization system, it is easy to estimate the size of some special objects, such as military targets, by just looking at the detail layer. Additional information about the image scene is also provided with interactive exploration tools. Overall, this technique can create informative displays in a succinct form to support practical decision making.

REFERENCES

- [1] T. M. Lillesand, R. W. Kiefer, and J. W. Chipman, *Remote Sensing and Image Interpretation*, 5th ed. Hoboken, NJ: Wiley, 2003.
- [2] P. K. Robertson and J. F. O'Callaghan, "The application of perceptual color spaces to the display of remotely sensed imagery," *IEEE Trans. Geosci. Remote Sens.*, vol. 26, no. 1, pp. 49–59, Jan. 1988.
- [3] J. M. Durand and Y. H. Kerr, "An improved decorrelation method for the efficient display of multispectral data," *IEEE Trans. Geosci. Remote Sens.*, vol. 27, no. 5, pp. 611–619, Sep. 1989.
- [4] J. S. Tyo, A. Konsolakis, D. I. Diersen, and R. C. Olsen, "Principal-components-based display strategy for spectral imagery," *IEEE Trans. Geosci. Remote Sens.*, vol. 41, no. 3, pp. 708–718, Mar. 2003.
- [5] S. Cai, Q. Du, R. Moorhead, M. J. Mohammadi-Aragh, and D. Irby, "Noise-adjusted principal component analysis for hyperspectral remotely sensed imagery visualization," in *Proc. IEEE Vis. Conf. (Compendium)*, 2005, pp. 119–120.
- [6] Q. Du, N. Raksuntorn, S. Cai, and N. Younan, "Color representation and classification for hyperspectral imagery," in *Proc. Int. Geosci. and Remote Sens. Symp.*, 2006, pp. 537–540.
- [7] N. P. Jacobson and M. R. Gupta, "Design goals and solutions for display of hyperspectral images," *IEEE Trans. Geosci. Remote Sens.*, vol. 43, no. 11, pp. 2684–2693, Nov. 2005.
- [8] A. R. S. Marcal, "Automatic color indexing of hierarchically structured classified images," in *Proc. IEEE Geosci. Remote Sens. Symp.*, 2005, vol. 7, pp. 4976–4979.
- [9] R. Wessels, M. Buchheit, and A. Espeset, "The development of a high performance, high volume distributed hyperspectral processor and display system," in *Proc. IEEE Geosci. and Remote Sens. Symp.*, 2002, vol. 4, pp. 2519–2521.
- [10] R. M. Kirby, H. Marmanis, and D. H. Laidlaw, "Visualizing multivalued data from 2-D incompressible flows using concepts from painting," in *Proc. IEEE Vis. Conf.*, 1999, pp. 333–340.
- [11] C. Forsell, S. Seipel, and M. Lind, "Simple 3-D glyphs for spatial multivariate data," in *Proc. IEEE Symp. Inf. Vis.*, 2005, pp. 119–124.
- [12] A. A. Bokinsky, "Multivariate data visualization with data-driven spots," Ph.D. dissertation, Univ. North Carolina, Chapel Hill, 2003.
- [13] D. C. Heinz and C.-I. Chang, "Fully constrained least squares linear spectral mixture analysis method for material quantification in hyperspectral imagery," *IEEE Trans. Geosci. Remote Sens.*, vol. 39, no. 3, pp. 529–545, Mar. 2001.
- [14] T. Han, D. G. Goodenough, A. Dyk, and J. Love, "Detection and correction of abnormal pixels in Hyperion images," in *Proc. Int. Geosci. and Remote Sens. Symp.*, 2002, vol. 3, pp. 1327–1330.
- [15] R. C. Gonzalez and R. E. Woods, *Digital Image Processing*, 2nd ed. Englewood Cliffs, NJ: Prentice-Hall, 2002.
- [16] G. Wyszecki and W. S. Stiles, *Color Science: Concepts and Methods, Quantitative Data and Formulae*. New York: Wiley-Interscience, 2000.
- [17] D. H. Brainard, "Colorimetry," in *OSA Handbook of Optics: Fundamentals, Techniques, and Design*, vol. 1, M. Bass, Ed. New York: McGraw-Hill, 1995.
- [18] C. G. Healey, "Effective visualization of large multidimensional datasets," Ph.D. dissertation, Univ. British Columbia, Vancouver, BC, Canada, 1996.
- [19] A. R. Smith, "Color gamut transform pairs," *Comput. Graph.*, vol. 12, no. 3, pp. 12–19, 1978.
- [20] C. Ware, *Information Visualization*, 2nd ed. San Mateo, CA: Morgan Kaufmann, 2004.
- [21] P. Camppadelli, R. Schettini, and S. Zuffi, "A system for the automatic selection of conspicuous color sets for qualitative data display," *IEEE Trans. Geosci. Remote Sens.*, vol. 39, no. 10, pp. 2283–2286, Oct. 2001.
- [22] C. G. Healey and J. T. Enns, "Large datasets at a glance: Combining textures and colors in scientific visualization," *IEEE Trans. Vis. Comput. Graph.*, vol. 5, no. 2, pp. 145–167, Apr./Jun. 1999.
- [23] D. Hearn and M. P. Baker, *Computer Graphics With OpenGL*, 3rd ed. Englewood Cliffs, NJ: Prentice-Hall, 2004.
- [24] D. A. Keim, "Designing pixel-oriented visualization techniques: Theory and application," *IEEE Trans. Vis. Comput. Graph.*, vol. 6, no. 1, pp. 59–78, Jan.–Mar. 2000.
- [25] J. Abello and J. Korn, "MGV: A system for visualizing massive multidigraphs," *IEEE Trans. Vis. Comput. Graph.*, vol. 8, no. 1, pp. 21–38, Jan.–Mar. 2002.



Shangshu Cai (S'06) received the B.S. and M.S. degrees in electrical engineering (Special Class for the Gifted Young) from the University of Science and Technology of China, Hefei, in 2000 and 2003, respectively. He is currently working toward the Ph.D. degree at Mississippi State University, Mississippi State.

His research interests include scientific visualization, high-dimensional data visualization, hyperspectral image displaying, and image processing.



Qian Du (S'98–M'00–SM'05) received the Ph.D. degree in electrical engineering from the University of Maryland Baltimore County, Baltimore, in 2000.

From 2000 to 2004, she was with the Department of Electrical Engineering and Computer Science, Texas A&M University—Kingsville. In fall of 2004, she joined the Department of Electrical and Computer Engineering, Mississippi State University, Mississippi State, where she is currently an Assistant Professor. Her research interests include remote sensing image analysis, pattern classification, data

compression, and neural networks.

Dr. Du is a member of SPIE, ASPRS, and ASEE.



Robert J. Moorhead, II (S'81–M'85–SM'92) received the B.S.E.E. degree from Geneva College, Beaver Falls, PA, in 1980 and the M.S.E.E. and Ph.D. degrees from North Carolina State University, Raleigh, in 1982 and 1985, respectively, all in electrical engineering.

He is currently a Professor in the Department of Electrical and Computer Engineering, Mississippi State University, Mississippi State, and an Associate Director of the GeoResources Institute. He was previously employed as a Research Staff Member

with the IBM T.J. Watson Research Center. His current research interests include computationally demanding visualization and analysis issues. He has previously conducted research in computer communications and image/video coding. He has published more than 100 papers.